Analysis of Photoirradiated Water Accommodated Fractions of Crude Oils Using Tandem TIMS and FT-ICR MS

Paolo Benigni,[†] Kathia Sandoval,[†] Christopher J. Thompson,[‡] Mark E. Ridgeway,[‡] Melvin A. Park,[‡] Piero Gardinali,[†,§] and Francisco Fernandez-Lima*[,†,‖]

[†]Department of Chemistry and Biochemistry, [§]Southeast Environmental Research Center, and [‖]Biomolecular Sciences Institute, Florida International University, Miami, Florida 33199, United States

[‡]Bruker Daltonics, Inc., Billerica, Massachusetts 01821, United States

Ⓢ Supporting Information

ABSTRACT: For the first time, trapped ion mobility spectrometry (TIMS) in tandem with Fourier transform ion cyclotron resonance mass spectrometry (FT-ICR MS) is applied to the analysis of the low energy water accommodated fraction (WAF) of a crude oil as a function of the exposure to light. The TIMS-FT-ICR MS analysis provided, in addition to the heteroatom series identification, new insights into the WAF isomeric complexity (e.g., $[m/z;$ chemical formula; collision cross section] data sets) for a better evaluation of the degree of chemical and structural photoinduced transformations. Inspection of the $[m/z;$ chemical formula; collision cross section] data sets shows that the WAF composition changes as a function of the exposure to light in the first 115 h

by initial photosolubilization of HC components and their photo-oxidation up to O_{4-5} of mainly high double bond equivalence species (DBE > 9). The addition of high resolution TIMS (resolving power of 90−220) to ultrahigh resolution FT-ICR MS (resolving power over 400k) permitted the identification of a larger number of molecular components in a single analysis (e.g., over 47k using TIMS-MS compared to 12k by MS alone), with instances of over 6-fold increase in the number of molecular features per nominal mass due to the WAF isomeric complexity. This work represents a stepping stone toward a better understanding of the WAF components and highlights the need for better experimental and theoretical approaches to characterize the WAF structural diversity.
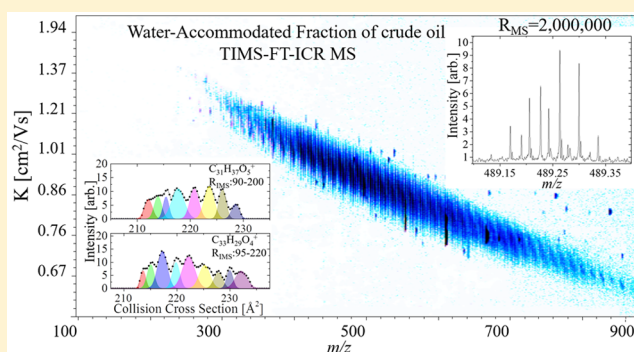
■ INTRODUCTION

The complex nature of crude oil and its incorporation in aquatic systems results in complex chemical transformations mainly via bio-[1−8] and photo degradation.[9−14] Natural and anthropogenic release of crude oil and hydrocarbons[15,16] to seawater is a frequent process, and recent studies have highlighted the importance of characterizing released crude oil at the molecular level.[17] For example, the characterization of heteroatom (O, N, and S) polyaromatic hydrocarbons (h-PAHs) has exhibited increased levels of toxicity compared to pure hydrocarbons.[18] Moreover, PAHs are photo active, undergoing oxygenation upon exposure to light, which can lead to chemical products that have increased biological accumulation and activity.[19−25] The presence of crude oil in water provides the means for the exposure of a large number of molecules to chemical and enzymatic transformation and their transportation across environments,[26−28] as well as the interaction with a variety of organisms.[26] Many of these chemical changes, as well as the means of exposure to organisms, occur in the water accommodated fraction, where low energy mixing introduces components of the oil into the water, without the formation of detectable emulsions.[29] The

main analytical challenge during the analysis of the low energy water accommodated fraction (WAF) remains the identification and quantitation of both the primary molecular species, as well as the transformation intermediates and products.

Over the past years, most of the efforts for the WAF analysis have been focused on the use of gas chromatography−mass spectrometry (GC-MS)[7,9,10,13,30−36] and two-dimensional gas chromatography (GCXGC-MS) with heavy standards.[31,37] While progress has been made in the WAF characterization, these approaches are limited to the volatility range of molecules that can be analyzed by GC, which typically excludes large and highly polar molecules.[38] These analytical limitations narrow the type of studies that can be performed and our understanding of the crude oil transformations in seawater since the molecular species that are inaccessible or form unresolvable "humps", known as the unresolved complex mixture (UCM), can make up most of the WAF content.[39,40] The analytical

challenges associated with the molecular characterization of the UCM has led to the use of alternative tools in order to unravel its chemical complexity. For example, studies utilizing ultrahigh mass resolution mass spectrometry (e.g., FT-ICR MS)[41−44] have enabled the identification of chemical formulas using the isotopic resolution and the high mass accuracy (sub ppm) with a variety of atmospheric pressure ionization sources (e.g., electrospray ionization, ESI,[45,46] atmospheric pressure chemical ionization, APCI,[47−49] atmospheric pressure photoionization, APPI,[50−53] and atmospheric pressure laser ionization, APLI[54−61]). The use of a variety of atmospheric pressure ionization sources has enabled, in turn, the study of different molecular fractions at the molecular level and has provided evidence of the high structural diversity of the WAF components in their functional groups, aromaticity, and polarity.[62−64]

The high structural diversity of the WAF samples has prompted the need to complement ultrahigh resolution mass analysis (e.g., FT-ICR MS measurements) with preseparation techniques (e.g., liquid and gas chromatography), in order to better discriminate the components along a second axis of separation, permitting some isomeric separation and increasing the dynamic range of the FT-ICR MS measurement.[59,60,65−69] However, the biggest challenge in the coupling of liquid and gas chromatography is that it limits the FT-ICR MS analysis time, and thus the ability to better separate isobaric species, due to the slow acquisition rates needed for ultrahigh resolution mass acquisitions.[48,65] Alternatively, other postionization, gas-phase separations have been proven to be a better match for FT-ICR MS analysis.[70−79] In particular, ion mobility spectrometry (IMS) presents many advantages for the analysis of complex mixtures, providing orthogonal separation to FT-ICR MS that is based on the tridimensional structure of the molecule.[80−82] Initial work showed the potential of IMS-MS analysis for the characterization of complex hydrocarbon mixtures using complementary IMS-MS and FT-ICR MS measurements (e.g., IMS-TOF MS and FT-ICR MS of the same sample).[83−92] More recently, with the development of trapped ion mobility spectrometry (TIMS),[93−95] several reports have shown the potential of TIMS-MS to decouple the mobility (K) separation from the MS analysis time for fast, gas-phase separation and for molecular structural elucidation.[51,93,96−117] In particular, the advantages of TIMS over traditional IMS analyzers have been shown for fast screening[96] and targeted[79] analysis of molecular ions from complex chemical mixtures; the study of isomerization kinetics of small molecules,[98] peptides, DNA, proteins, and their complexes in the absence of the bulk solvent;[99−103] the influence of the collision partner on the molecular structure;[104] and the factors that affect molecular-adduct complex lifetime and stability during TIMS measurements.[105] A significant feature to note is the high resolving power of TIMS analyzers (R_{TIMS} up to 400[107]) and accuracy in measuring ion-neutral collision cross section (CCS, < 0.6% error). In the case of crude oils and complex mixtures, their characterization by TIMS-FT-ICR MS has allowed the measurement of the CCS, accurate mass, and accurate isotopic fine structure in a single experiment for a series of h-PAHs. For example, a recent report of Oversampling Selective Accumulation Trapped Ion Mobility Spectrometry (OSA-TIMS) coupled to FT-ICR MS showed high mobility resolving powers (over 250), high mass accuracy (<1 ppm), and ultrahigh mass resolution (up to 1,200,000 at m/z 400) during the analysis of a

complex mixture of polyaromatic hydrocarbons (PAH) from coal tar.[106]

In the present work, for the first time, we apply tandem OSA-TIMS and FT-ICR MS for the analysis of WAF samples as a function to their exposure to light. While preliminary work has shown that WAF can undergo chemical transformations and increase oil solubilization as a function to the exposure to light,[43] little is known about the WAF structural variability and transformation pathways. In this study, as an initial step, the analysis focuses on the PAH compounds accessible to ionization by an APLI source (e.g., mostly conjugated molecules) which typically exhibits higher reactivity to light resulting in more hazardous byproducts.[118] In addition to the new analytical advantages of TIMS-FT-ICR MS, a Software Assisted Molecular Elucidation (SAME) package was developed for the unsupervised processing of the OSA-TIMS-FT-ICR MS data sets. As shown below, this work highlights the need for high mobility resolution and ultrahigh resolution MS for the analysis of the highly isomeric, complex WAF mixtures while providing [m/z; chemical formula; K; CCS] in a single experiment.

■ EXPERIMENTAL SECTION

Sample Preparation. Low-energy water accommodated fractions (WAF) were generated according to the standardized protocol established by the Chemical Response to Oil Spills: Ecological Research Forum (CROSERF).[119,120] Briefly, WAFs were prepared at room temperature in 2-L aspirator bottles with 20% headspace by volume using artificial filtered saltwater (pore size: 0.45 μm, salinity = 33 parts-per-thousand) prepared with Instant Ocean (Aquarium Systems, Mentor OH). Oil from the Marlin Platform was added to the water surface using a gastight syringe at an oil-to-water loading of 1:1000 (1 g oil/L seawater). The bottles were covered in aluminum foil and allowed to mix for 24 h at low speed (100 rpm) in the dark.

WAF Exposure to Light and Extraction. WAF samples were irradiated up to 115 h with a Suntest XLS+ Sunlight Exposure System equipped with a 1500W xenon arc lamp and light intensity of 765 W/m^2 (Atlas, Chicago, IL, USA). The aspirator bottles containing the WAF and the oil were placed in a water bath system set to 25 °C. At specific irradiation times (0, 16, and 115 h), 150 mL aliquots of the WAF were removed and subjected to liquid−liquid extraction in three 50 mL lots of methylene chloride to increase extraction efficiency. Aliquots were dried over Na$_2$SO$_4$ and concentrated down to 1 mL under a stream of nitrogen. The final samples were then diluted 1:100 in 1:1 v/v methanol/toluene for FT-ICR MS and TIMS-FT-ICR MS analysis.

FT-ICR MS Analysis. WAF samples were analyzed in positive ion mode with an APLI source coupled to a custom-built TIMS − FT-ICR MS instrument based on the 7T Solarix FT-ICR MS spectrometer (Bruker Daltonics Inc., MA). Briefly, the APLI source utilizes a 266 nm excimer laser (CryLas GmbH, Berlin, Germany; Type:1HP266-50); the sample was introduced at 200 μL/h through a short nebulizer in a vaporizer set to 300 °C into the source chamber where the gas stream was ionized by the excimer laser.[65] The APLI generates radical ([M]$^{+\bullet}$) and protonated ([M + H]$^+$) ions in the source region that are introduced to the TIMS-FT-ICR MS via a 0.6 mm inner diameter, single-bore resistive glass capillary tube, allowing the nebulizer to be maintained at ground potential, while the ends of the capillary can be independently biased. Typical APLI operating conditions were 1 L/min dry gas flow
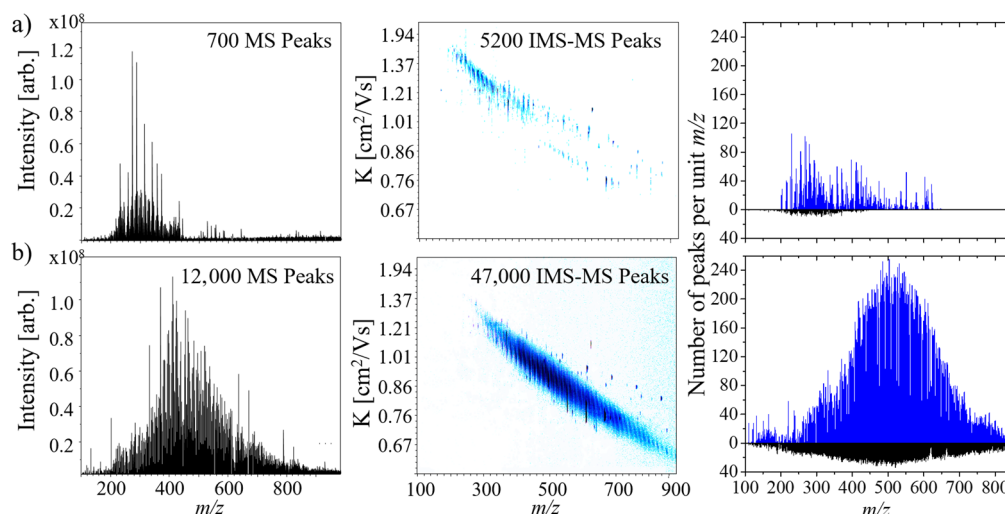
Figure 1. Typical FT-ICR MS spectrum and 2D TIMS-FT-ICR MS contour plot for the WAF (a) at 0 and (b) 115 h light exposed. The number of peaks identified per unit m/z in the MS domain (black) and TIMS-MS (blue) domains are also shown for (a) and (b). Notice the significant differences in the number of identifications between (a) and (b), as well as between the MS and TIMS MS experiments, increasing the level of molecular features identified per analysis.

rate, 2.1 bar nebulizer gas pressure, and 220 °C dry gas temperature. FT-ICR MS ion optics were optimized as follows: −900 V end-cap source capillary voltage, 180 V end-cap TIMS capillary voltage, 5 kHz 400 peak-to-peak voltage (Vpp) segmented hexapole, 2 kHz 1900 Vpp collision cell, and 4 kHz 400 Vpp ion guide transfer line. The FT-ICR MS experiments were performed by coadding 200 16 Megaword (8 s) transients, which were zero-filled to 32Megaword, processed using a half-sine apodization followed by fast-Fourier transform (FFT) and broadband phase correction (absorption spectra using absorption mode processing, AMP); an experimental MS resolving power with AMP at m/z 400 of ~2,000,000 was obtained.

TIMS-FT-ICR MS Analysis. The concept behind TIMS is the use of an electric field to hold ions stationary against a moving gas, so that the drag force is compensated by the electric field and ion packages are separated across the TIMS analyzer axis based on their mobility.[93−95] During mobility separation, a quadrupolar field confines the ions in the radial direction to increase trapping efficiency. A simplified schematic of a TIMS analyzer is shown in the Supporting Information (Figure S1). The mobility, K, of an ion in a TIMS cell is described by

$$K = \frac{v_g}{E} = \frac{A}{(V_{elution} - V_{out})} \quad (1)$$

where v_g, E, $V_{elution}$, and V_{out} are the velocity of the gas, applied electric field, elution voltage, and tunnel out voltage, respectively. TIMS separation was performed using nitrogen as a bath gas at ca. 300 K, front end $P_1 = 3.0$ and back end $P_2 = 1.1$ mbar pressures, a constant $V_{out} = 35$ V and constant RF (840 kHz and 240 Vpp) in all electrodes of the entrance funnel, mobility separating section, and exit funnel. Details regarding Oversampling Selected Accumulation TIMS (OSA-TIMS) modes of operation[106] and specifics compared to traditional TIMS and IMS can be found elsewhere.[93−96,98] Briefly, OSA-TIMS experiments were performed by scanning V_{in} from −40 to −210 V using a 1 V ramp size and 0.2 V increments per step, accumulating 40 mobility experiments per FT-ICR MS spectrum (4Megaword, 3s transient, with six transients coadded

per MS). TIMS-FT-ICR MS spectra were processed using sine-squared apodization followed by FFT, in magnitude mode resulting in an experimental MS resolving power of $R \sim$ 400,000 at m/z 400. Mobility spectra were calibrated using a Tuning Mix calibration standard (Tunemix, G2421A, Agilent Technologies, Santa Clara, CA) with the following reduced mobility (K_0) values m/z 622 $K_0 = 1.025$, m/z 922 $K_0 = 0.840$, m/z 1222 $K_0 = 0.724$, m/z 1522 $K_0 = 0.643$ cm^2 V^{-1} s^{-1}. Mobilities were correlated with CCS (Ω) using the equation

$$\Omega = \frac{(18\pi)^{1/2}}{16} \frac{z}{(k_B T)^{1/2}} \left[\frac{1}{m_I} + \frac{1}{m_b} \right]^{1/2} \frac{1}{K} \frac{760}{P} \frac{T}{273.15} \frac{1}{N^*} \quad (2)$$

where z is the charge of the ion, k_B is the Boltzmann constant, N^* is the number density, and m_I and m_b refer to the masses of the ion and bath gas, respectively.[121] Under these conditions, the experimental TIMS resolving power for Tuning Mix (m/z 622−1522) was ~100−250 as determined by eq 3.

$$R = \frac{\Omega}{\Delta\Omega} \quad (3)$$

Data Processing. FT-ICR MS spectra were externally mass calibrated using the Tuning Mix standard. A peak list was generated allowing a signal-to-noise ratio of 6, and the data were internally recalibrated (postacquisition) using a double bond equivalence of 9 O_1 series to improve overall mass accuracy.[122] The formulas calculations from the exact mass domain were performed using Composer software (Version 1.0.6, Sierra Analytics, CA) and confirmed with Data Analysis (Bruker Daltonics v 4.2) using formula limits of $C_{1-100}H_{1-100}N_{0-2}O_{0-10}S_{0-2}$, odd and even electron configurations were allowed, and M$^{+\bullet}$ and [M + H]$^+$ ion forms. While the oxygen content was limited to ten oxygen atoms in the initial search, molecular matches with more than six oxygen atoms were not observed; we interpret the low number of oxygen content as a consequence of the shorter irradiation time when compared to previously reported experiments. A root-mean-square deviation for the mass assignments of 0.3 ppm was
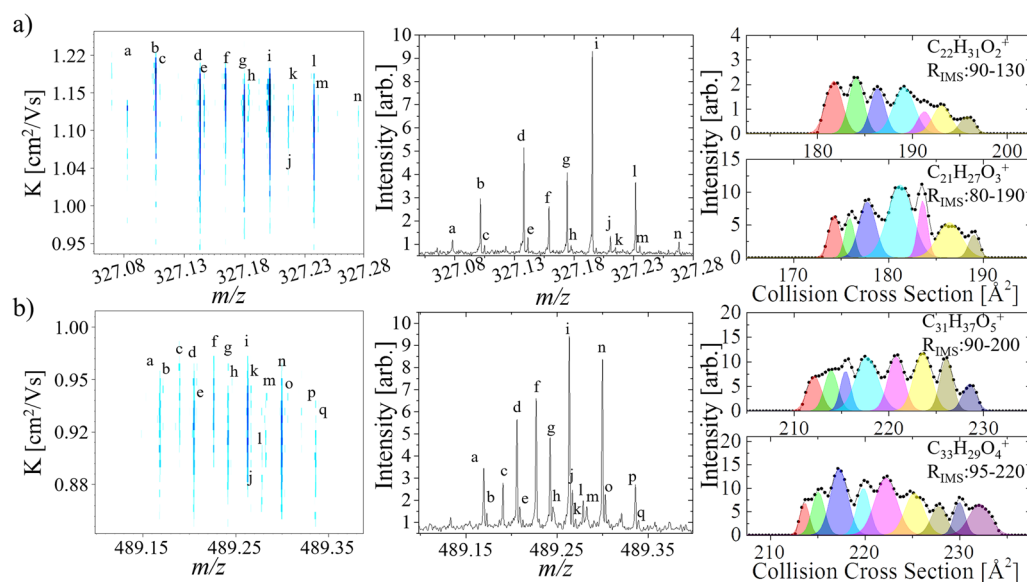
Figure 2. Typical 2D TIMS-FT-ICR MS contour plot and MS projections for *m/z* a) 327 and b) 489. IMS projections for specific chemical formulas (connected scatterplot) with the unsupervised fitting by the SAME package of minimum number of mobility features is shown. Note that the SAME package relies on the experimental profile of the distribution, which is able to show multiple features due to the high resolving power of the TIMS analyzer. Formula assignments are provided in Table 1.

observed. From the generated ion formulas, the double bond equivalence (DBE) was calculated by the equation

$$DBE = C - \frac{H}{2} + \frac{N}{2} + 1 \tag{4}$$

where *C*, *H*, and *N* are the number of carbons, hydrogens, and nitrogens in the chemical formula.

The peak list was used for extraction of the ion mobility spectra from the TIMS-FT-ICR MS data sets using batch processing in the Data Analysis package (Version v. 4.2, Bruker Daltonics, CA) followed by external mobility calibration using the Tuning Mix standards. The TIMS spectrum for each molecular formula was processed using a custom-built Software Assisted Molecular Elucidation (SAME) package—a specifically designed 2D TIMS-FT-ICR MS data processing script written in Python v2.7. The SAME package utilizes noise removal, mean gap filling, "asymmetric least squares smoothing" baseline correction,[70] peak detection by continuous wavelet transform (CWT)-based peak detection algorithm (SciPy package),[123,124] and Gaussian fitting with nonlinear least-squares functions (Levenberg–Marquardt algorithm).[125] SAME final outcome is [*m/z*; chemical formula; K; CCS] for each 2D TIMS-FT-ICR MS data set. The 2D TIMS-FT-ICR MS contour plots were generated in DataAnalysis (Version v. 4.2, Bruker Daltonics, CA), and all the other plots were generated using matplotlib[126] and OriginPro 2016 (Originlab Co., MA).

■ RESULTS AND DISCUSSION

The analysis of the WAF samples by APLI-FT-ICR MS can be characterized by a Gaussian-like distribution, centered at *m/z* 300 (Figure 1). Prior to exposure to light (t-0h), ~700 peaks were observed in the FT-ICR MS spectra. After the WAF was exposed to light (t-115h), the distribution increased in size, and the center shifted to *m/z* 500, resulting in ~12,000 peaks, which represents an ~17-fold increase relative to the unexposed WAF (t-0h). The change in the MS distribution suggests an increased partitioning of the oil in the WAF (e.g., photo-solubilization) as well as potential chemical transformations

within the WAF as a function of the exposure to light. The use of an ultrahigh resolution mass analyzer allowed the assignment of chemical formulas and to track changes in the WAF as a function of the exposure to light (see Figures S2−S4). By using an APLI source there is an intrinsic bias on the type of molecular ions that can be produced and may result in a lower number of potential features identified from the WAF sample. However, closer inspection to the observed features shows a high chemical diversity and complexity, comparable to those observed using other ionization sources.[41] A follow up analysis using OSA-TIMS in tandem with FT-ICR MS enabled further molecular separation of the WAF content by their mobility (isomeric content) followed by ultrahigh resolution mass analysis. For example, the number of molecular features increased from ~700 to ~5.2k and from ~12k to ~47k for the t-0h and t-115h WAF samples, respectively, by adding the TIMS separation to the FT-ICR MS analysis. Moreover, the isomeric content of the WAF samples is such that TIMS separation increases the number of features up to 6-fold at the nominal level (see Figure 1). That is, OSA-TIMS in tandem with FT-ICR MS enabled a more comprehensive analysis of the WAF content by increasing the peak capacity of the analysis using complementary, orthogonal TIMS and FT-ICR MS separations.

Inspection of the 2D-TIMS-FT-ICR MS contour plots indicated that the observed chemical species from the WAF samples using the APLI source are mostly condensed/aromatic molecules (see more details on interpreting 2D-IMS-MS contour plots in ref 106). This observation is consistent with previous analysis using APLI sources that showed better ionization efficiencies for molecules containing conjugated bonds.[65] Closer inspection of the 2D TIMS-FT-ICR MS WAF data reveals the spectral complexity in both the mass and mobility dimensions. Particularly, the presence of multiple isobaric interferences (e.g., -C$_3$ to -SH$_4$ splits, Δ*m* = 3.4 mDa, requiring ~150,000 resolving power at *m/z* 489), such as C$_{31}$H$_{37}$O$^+$, C$_{28}$H$_{41}$OS$^+$, C$_{25}$H$_{45}$OS$_2$$^+$, as well as multiband ion mobility projections confirm the need for high resolution TIMS

analysis during the study of the WAF samples (TIMS resolving power up to 220 is shown in Figure 2). While the SAME package is designed to fit the mobility profiles and to provide a minimum number of IMS peaks, inspection of Figure 2 shows that coelution may be observed in the ion mobility dimension due to the high sample complexity; in the case shown, restrictions to the peak width fitting in the SAME package were not imposed in order to better account for the structural flexibility of potential isomers. For example, at m/z 327, 14 MS peaks are detected and chemical formulas are assigned (see Table 1). For each chemical formula, an extracted ion mobility

Table 1. Table of Identified Ion Formulas for m/z 327 and 489 as Found in Figure 2

m/z		exp. m/z	ion formula	error (ppb)
327	a	327.078031	$C_{15}H_{21}NOS_3^+$	−159
	b	327.101557	$C_{22}H_{15}O_3^+$	43
	c	327.104917	$C_{19}H_{19}O_3S^+$	76
	d	327.137957	$C_{23}H_{19}O_2$	−3
	e	327.141345	$C_{20}H_{23}O_2S^+$	−55
	f	327.159052	$C_{20}H_{23}O_4^+$	104
	g	327.174325	$C_{24}H_{23}O^+$	52
	h	327.177623	$C_{21}H_{27}OS^+$	275
	i	327.195425	$C_{21}H_{27}O_3^+$	141
	j	327.210673	$C_{25}H_{27}^+$	165
	k	327.214774	$C_{22}H_{31}S^+$	−2066
	l	327.231822	$C_{22}H_{31}O_2^+$	107
	m	327.235269	$C_{19}H_{35}O_2S$	−125
	n	327.268202	$C_{23}H_{35}O^+$	122
489	a	489.169661	$C_{32}H_{25}O_5^+$	−22
	b	489.172941	$C_{29}H_{29}O_5S^+$	164
	c	489.190592	$C_{29}H_{29}O_7$	384
	d	489.205937	$C_{33}H_{29}O_4^+$	202
	e	489.209127	$C_{30}H_{33}O_4S^+$	572
	f	489.227101	$C_{30}H_{33}O_6^+$	131
	g	489.242320	$C_{34}H_{33}O_3^+$	206
	h	489.245496	$C_{31}H_{37}O_3S^+$	605
	i	489.263445	$C_{31}H_{37}O_5^+$	217
	j	489.266855	$C_{28}H_{41}O_5S^+$	137
	k	489.270311	$C_{25}H_{45}O_5S_2^+$	−37
	l	489.278685	$C_{35}H_{37}O_2^+$	249
	m	489.282768	$C_{32}H_{41}O_2S^+$	−1206
	n	489.299809	$C_{32}H_{41}O_4^+$	260
	o	489.302875	$C_{29}H_{45}O_4S^+$	883
	p	489.336155	$C_{33}H_{45}O_3^+$	341
	q	489.339652	$C_{30}H_{49}O_3S^+$	84

chromatogram was generated, resulting in 47 peaks with assigned chemical formula, mobility, and CCS. Notice that this detailed separation is only possible due to the high resolving power of the TIMS device, the OSA-TIMS method providing sufficient points across the mobility profile, and the ultrahigh resolution and mass accuracy of the FT-ICR MS. Moreover, the processing of the 2D-TIMS-FT-ICR MS data using the SAME package is able to deconvolute the mobility profile in a minimum number of isomers (see examples for $C_{22}H_{31}O_2^+$ and $C_{21}H_{27}O_3^+$ in Figure 2). A similar complexity can be observed at m/z 489, where 17 peaks are resolved in the FT-ICR MS and 123 peaks in the 2D TIMS-FT-ICR MS. The time independent nature of the OSA-TIMS analysis permits the acquisition of high mass resolution FT-ICR MS spectra, thus maximizing the analytical potential of both techniques while providing precise

collision cross section (less than 1% variability between replicates). It should be pointed out that these results provide a new reference point for the IMS-MS analysis; commonly accessible IMS-MS platforms are limited to IMS resolving power of ∼30−60 (with instances up to 100) and to TOF MS detectors with MS resolving power up to 60k.[83−91]

Taking advantage of the high mobility resolution and ultrahigh mass separation of TIMS-FT-ICR MS, the WAF $[m/z;$ chemical formula; K; CCS] components can be followed as a function of the exposure to light for each chemical class (see example in Figure 3). The increase in the number of molecular species from the HC class as a function of the exposure to light suggests that WAF is initially subject to photosolubilization of the surface slick into the water, in good agreement with previous observations.[41] Results from the HC class show that the increase in the DBE is associated with a reduction in the CCS for a given carbon number. For example, for C_{34} the lowest CCS of 210 Å^2 corresponds to DBE 14, while DBE 5 has the greatest CCS of 252 Å^2. This indicates that the degree of condensation (e.g., rings and double bonds) imposes structural boundaries, reducing the CCS of a molecule.[85,127] In addition to the initial photosolubilization, as the exposure of the WAF to light increases, a greater number of assignments with carbon numbers greater than 40 are observed, particularly comparing 16 and 115 h. Furthermore, there is an increase in the number of oxygenated classes and a decrease in the HC class, especially for compounds with DBE > 9. In particular, the identified formulas for the O$_4$ and O$_5$ classes have DBE ranges between 8 and 20, and 9 and 18, and occupy a narrow structural space in the condensed region of the mobility domain, which may indicate that these are products of the higher photosensitive and reactive aromatic HC structures.[128] Although the WAF transformation mechanisms are not well understood, our results suggest that the photo-transformation of the HC molecules in WAF leads to the observation of oxygenated species of the O$_{4−5}$ class in the first 115h of exposure to light.

Changes in the WAF composition can be also followed by the presence of specific chemical formulas as a function of the exposure to light. For example, inspection of the WAF $[m/z;$ chemical formula; K; CCS] components at different time points can be used to infer the degree of chemical transformations (see Figure 4). For example, the unexposed WAF, t-0h, has few identifications for the HC class (black bars); however, at t-16h (red bars) there is a significant increase in the number of assignments, 420 new identifications based on MS alone and 3000 based on TIMS-MS followed by a decrease in the number of nonoxygenated molecules (e.g., HC and N class molecules) at t-115h.[43] This result suggests that there are several chemical transformations occurring as a consequence of the photosolubilization of the surface oil (e.g., indicated by the new identifications for the HC class at t-115h) and increased oxygenation of previously dissolved WAF components (e.g., the 3-fold increase in the number of identifications for the O$_3$ class and the appearance of the O$_4$ and O$_5$ classes with 1140 and 420 identifications, respectively). The oxygenated molecules are also highly isomeric, with up to 9 ion mobility bands per chemical formula. The observation of the O$_{4−5}$ classes at later irradiation times (t-115h) suggests that these molecules were not originally present in the WAF but are a consequence of the oxygenation process that took place over time, either by the generation of new molecules or by a decrease in matrix effects due to a lower number of UV absorbent molecules. That is, a
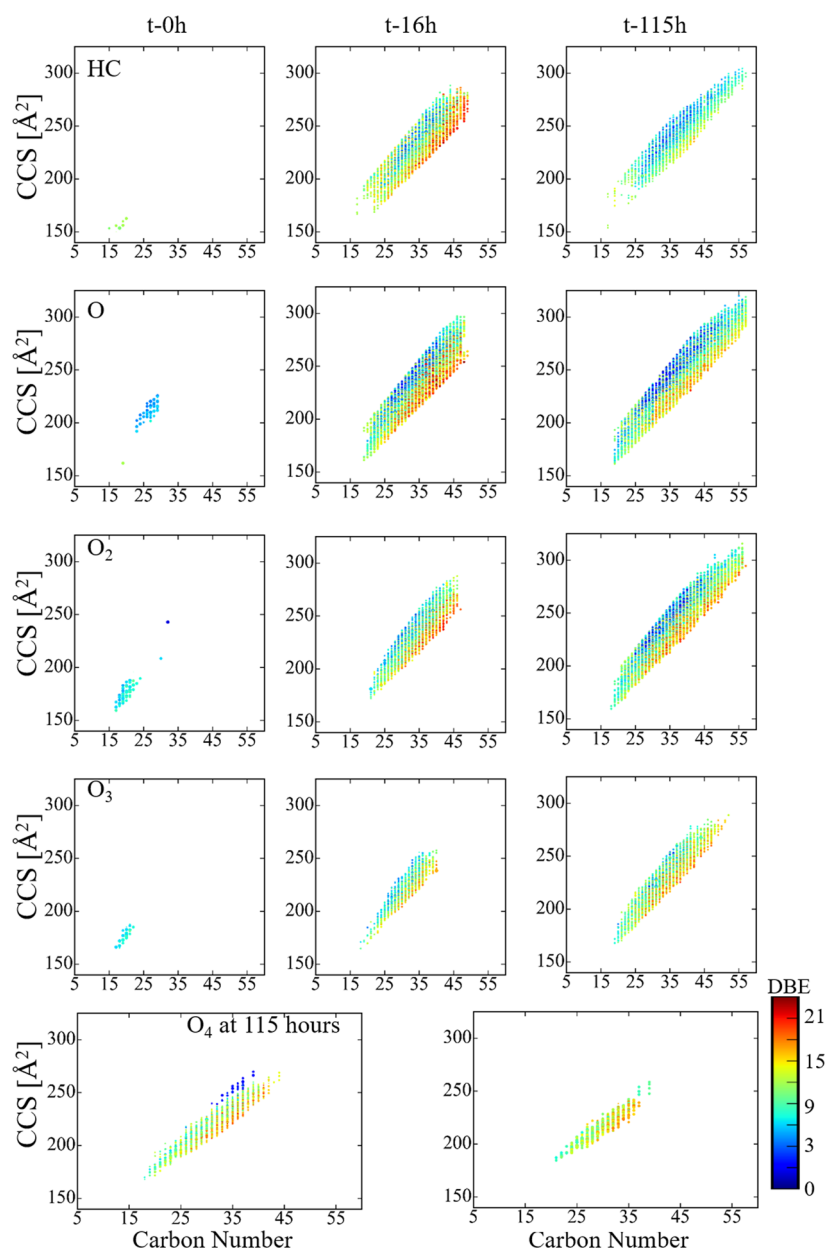
Figure 3. Typical size dependence (CCS) with carbon number for the O_{0-4} chemical classes observed in the WAF samples as a function to exposure to light (t-0h, -16h, and -115h). The color scale corresponds to the number of rings and double bond equivalents (DBE) of a molecule. Note the large increase in assignments between t-0h and t-16h, as well as increases in oxygen content between t-16h and t-115h.

reduction of molecules that are highly absorbent of the 266 nm excimer laser may result in greater sensitivity for less absorbent and low concentration molecules. Note that the increase in oxygenation is in good agreement with other MS reports of WAF exposure to light.[129,130] Small differences were observed between the number of identifications, such as the HC class, by TIMS-MS and MS alone due to the reduced TIMS trapping efficiency for low m/z ions and low abundant ions when performing a broad range mobility analysis; however, this limitation can be overcome by performing targeted analysis for smaller PAHs (e.g., naphthalene) as previously reported.[96]

This work showcases the unique advantages of OSA-TIMS in tandem with FT-ICR MS and represents a major step toward the analytical characterization (i.e., high mobility resolving power over 220 combined with ultrahigh mass resolution over 400k) of WAF samples at the molecular level in a single

experiment. While these preliminary experiments address one part of a complex environmental challenge (e.g., APLI accessible molecular ions from WAF) and showcase a major improvement in the way we can analytically describe the molecular composition and structural diversity of the WAF, further experiments and developments are needed in order to better understand the environmental implications and the structure–function relationship of the WAF components. For example, a more complete characterization of the WAF content and their transformation products and intermediates will require the use of a suite of ionization sources, in both positive and negative polarities, in order to cover a larger range of chemical species during the analysis.[62,131] Further interpretation of the WAF [m/z; chemical formula; K; CCS] components can be made with the use of standards, theoretical calculations of candidate structures,[79,96,97] and the implementa-
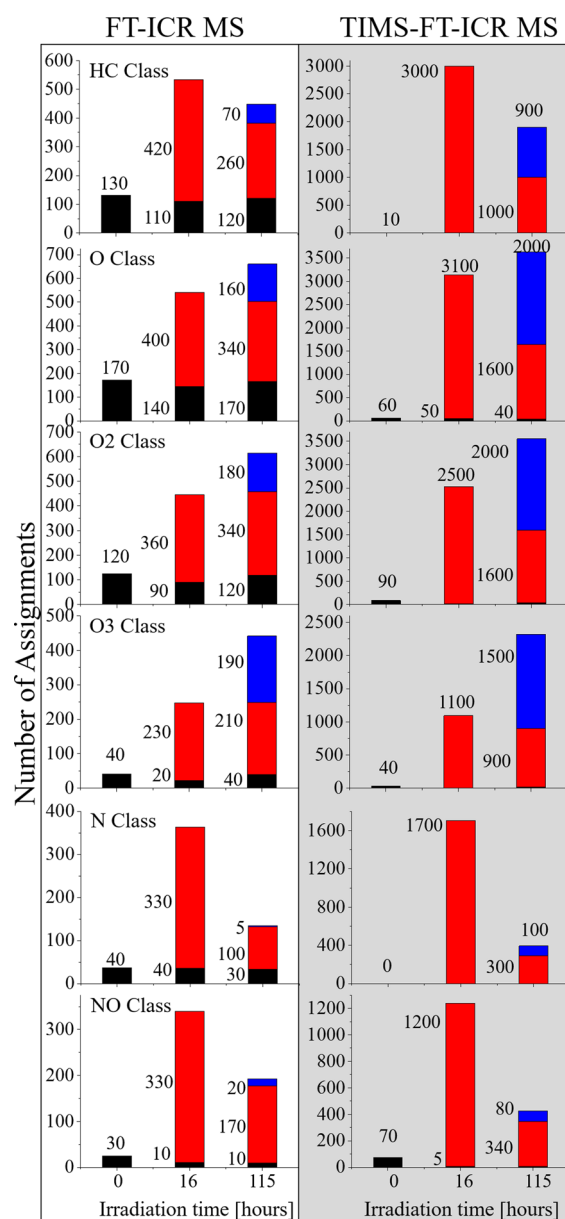
Figure 4. Total number of molecular feature assignments based on chemical formula alone from FT-ICR MS measurements and based on chemical formula and IMS profiling from TIMS-FT-ICR MS measurements. Identifications unique to t-0, t-16, and t-115h are in black, red, and blue, respectively. When FT-ICR MS is used tracing the evolution of the chemical complexity is incomplete, because the isomeric complexity is not taken into account. Particularly, taking into account the isomeric variability indicates that the composition of the WAF at t-115h is significantly more complex, and chemically unique, than is observed by FT-ICR MS alone.

tion of complementary, postionization MS structural tools in tandem with TIMS-FT-ICR MS (e.g., MS/MS using CID, SID, IRMPD, BIRD, ExD, etc.)[132−138] Although initial attempts have been made toward the structural characterization,[97] the 2D TIMS-FT-ICR MS data sets contain a large amount of analytical data (e.g., over 50k features) in need of further development of theoretical "petro-informatics" and computational approaches capable of producing more detailed structural information on the WAF phototransformation products and intermediates.

■ **AUTHOR INFORMATION**

Corresponding Author

*Phone: 305-348-2037. Fax: 305-348-3772. E-mail: fernandf@fiu.edu.

ORCID ⓘ

Francisco Fernandez-Lima: 0000-0002-1283-4390

Notes

The authors declare no competing financial interest.

■ **REFERENCES**

(1) Ghosal, D.; Ghosh, S.; Dutta, T. K.; Ahn, Y. Current state of knowledge in microbial degradation of polycyclic aromatic hydrocarbons (PAHs): a review. *Front. Microbiol.* **2016**, *7*, 1369.

(2) Kanaly, R. A.; Harayama, S. Biodegradation of high-molecular-weight polycyclic aromatic hydrocarbons by bacteria. *J. Bacteriol.* **2000**, *182* (8), 2059−2067.

(3) Haritash, A. K.; Kaushik, C. P. Biodegradation aspects of polycyclic aromatic hydrocarbons (PAHs): a review. *J. Hazard. Mater.* **2009**, *169* (1−3), 1−15.

(4) King, G. M.; Kostka, J. E.; Hazen, T. C.; Sobecky, P. A. Microbial responses to the Deepwater Horizon oil spill: from coastal wetlands to the deep sea. *Ann. Rev. Mar Sci.* **2015**, *7* (1), 377−401.

(5) Venosa, A. D.; Zhu, X. Q. Biodegradation of crude oil contaminating marine shorelines and freshwater wetlands. *Spill Sci. Technol. Bull.* **2003**, *8* (2), 163−178.

(6) Wang, J.; Sandoval, K.; Ding, Y.; Stoeckel, D.; Minard-Smith, A.; Andersen, G.; Dubinsky, E. A.; Atlas, R.; Gardinali, P. Biodegradation of dispersed Macondo crude oil by indigenous Gulf of Mexico microbial communities. *Sci. Total Environ.* **2016**, *557−558*, 453−468.

(7) Yang, Z. Y.; Hollebone, B. P.; Wang, Z. D.; Yang, C.; Brown, C.; Zhang, G.; Landriault, M.; Ruan, X. C. A preliminary study for the photolysis behavior of biodiesel and its blends with petroleum oil in simulated freshwater. *Fuel* **2015**, *139*, 248−256.

(8) Gutierrez, T.; Singleton, D. R.; Berry, D.; Yang, T.; Aitken, M. D.; Teske, A. Hydrocarbon-degrading bacteria enriched by the Deepwater Horizon oil spill identified by cultivation and DNA-SIP. *ISME J.* **2013**, *7* (11), 2091.

(9) D'Auria, M.; Emanuele, L.; Racioppi, R.; Velluzzi, V. Photochemical degradation of crude oil: Comparison between direct

irradiation, photocatalysis, and photocatalysis on zeolite. *J. Hazard. Mater.* **2009**, *164* (1), 32−8.

(10) Sabate, J.; Bayona, J. M.; Solanas, A. M. Photolysis of PAHs in aqueous phase by UV irradiation. *Chemosphere* **2001**, *44* (2), 119−24.

(11) Brame, J. A.; Hong, S. W.; Lee, J.; Lee, S. H.; Alvarez, P. J. Photocatalytic pre-treatment with food-grade TiO(2) increases the bioavailability and bioremediation potential of weathered oil from the Deepwater Horizon oil spill in the Gulf of Mexico. *Chemosphere* **2013**, *90* (8), 2315−9.

(12) Nicodem, D. E.; Fernandes, M. C. Z.; Guedes, C. L. B.; Correa, R. J. Photochemical processes and the environmental impact of petroleum spills. *Biogeochemistry* **1997**, *39* (2), 121−138.

(13) Maki, H.; Sasaki, T.; Harayama, S. Photo-oxidation of biodegraded crude oil and toxicity of the photo-oxidized products. *Chemosphere* **2001**, *44* (5), 1145−51.

(14) Lemkau, K. L.; McKenna, A. M.; Podgorski, D. C.; Rodgers, R. P.; Reddy, C. M. Molecular evidence of heavy-oil weathering following the M/V Cosco Busan spill: insights from Fourier transform ion cyclotron resonance mass spectrometry. *Environ. Sci. Technol.* **2014**, *48* (7), 3760−7.

(15) Lea-Smith, D. J.; Biller, S. J.; Davey, M. P.; Cotton, C. A.; Sepulveda, B. M. P.; Turchyn, A. V.; Scanlan, D. J.; Smith, A. G.; Chisholm, S. W.; Howe, C. J. Contribution of cyanobacterial alkane production to the ocean hydrocarbon cycle. *Proc. Natl. Acad. Sci. U. S. A.* **2015**, *112* (44), 13591−13596.

(16) Valentine, D. L.; Reddy, C. M. Latent hydrocarbons from cyanobacteria. *Proc. Natl. Acad. Sci. U. S. A.* **2015**, *112* (44), 13434−13435.

(17) Bacosa, H. P.; Erdner, D. L.; Liu, Z. Differentiating the roles of photooxidation and biodegradation in the weathering of Light Louisiana Sweet crude oil in surface water from the Deepwater Horizon site. *Mar. Pollut. Bull.* **2015**, *95* (1), 265−72.

(18) Lübcke-von Varel, U.; Machala, M.; Ciganek, M.; Neca, J.; Pencikova, K.; Palkova, L.; Vondracek, J.; Löffler, I.; Streck, G.; Reifferscheid, G.; Flückiger-Isler, S.; Weiss, J. M.; Lamoree, M.; Brack, W. Polar Compounds Dominate in Vitro Effects of Sediment Extracts. *Environ. Sci. Technol.* **2011**, *45* (6), 2384−2390.

(19) Lee, R. F. Photo-oxidation and photo-toxicity of crude and refined oils. *Spill Sci. Technol. Bull.* **2003**, *8* (2), 157−162.

(20) Duesterloh, S.; Short, J. W.; Barron, M. G. Photoenhanced toxicity of weathered Alaska North Slope crude oil to the calanoid copepods Calanus marshallae and Metridia okhotensis. *Environ. Sci. Technol.* **2002**, *36* (18), 3953−9.

(21) Barron, M. G.; Carls, M. G.; Heintz, R.; Rice, S. D. Evaluation of fish early life-stage toxicity models of chronic embryonic exposures to complex polycyclic aromatic hydrocarbon mixtures. *Toxicol. Sci.* **2004**, *78* (1), 60−67.

(22) Knecht, A. L.; Goodale, B. C.; Truong, L.; Simonich, M. T.; Swanson, A. J.; Matzke, M. M.; Anderson, K. A.; Waters, K. M.; Tanguay, R. L. Comparative developmental toxicity of environmentally relevant oxygenated PAHs. *Toxicol. Appl. Pharmacol.* **2013**, *271* (2), 266−75.

(23) Huang, X. D.; McConkey, B. J.; Babu, T. S.; Greenberg, B. M. Mechanisms of photoinduced toxicity of photomodified anthracene to plants: Inhibition of photosynthesis in the aquatic higher plant Lemna gibba (duckweed). *Environ. Toxicol. Chem.* **1997**, *16* (8), 1707−1715.

(24) Duxbury, C. L.; Dixon, D. G.; Greenberg, B. M. Effects of simulated solar radiation on the bioaccumulation of polycyclic aromatic hydrocarbons by the duckweed Lemna gibba. *Environ. Toxicol. Chem.* **1997**, *16* (8), 1739−1748.

(25) Lampi, M. A.; Gurska, J.; McDonald, K. I.; Xie, F.; Huang, X. D.; Dixon, D. G.; Greenberg, B. M. Photoinduced toxicity of polycyclic aromatic hydrocarbons to Daphnia magna: ultraviolet-mediated effects and the toxicity of polycyclic aromatic hydrocarbon photoproducts. *Environ. Toxicol. Chem.* **2006**, *25* (4), 1079−87.

(26) Mason, O. U.; Scott, N. M.; Gonzalez, A.; Robbins-Pianka, A.; Bælum, J.; Kimbrel, J.; Bouskill, N. J.; Prestat, E.; Borglin, S.; Joyner, D. C. Metagenomics reveals sediment microbial community response to Deepwater Horizon oil spill. *ISME J.* **2014**, *8* (7), 1464−1475.

(27) Gong, Y.; Zhao, X.; Cai, Z.; O'Reilly, S. E.; Hao, X.; Zhao, D. A review of oil, dispersed oil and sediment interactions in the aquatic environment: Influence on the fate, transport and remediation of oil spills. *Mar. Pollut. Bull.* **2014**, *79* (1−2), 16−33.

(28) Boglaienko, D.; Tansel, B. Partitioning of fresh crude oil between floating, dispersed and sediment phases: Effect of exposure order to dispersant and granular materials. *J. Environ. Manage.* **2016**, *175*, 40−45.

(29) Sandoval, K.; Ding, Y.; Gardinali, P. Characterization and environmental relevance of oil water preparations of fresh and weathered MC-252 Macondo oils used in toxicology testing. *Sci. Total Environ.* **2017**, *576*, 118−128.

(30) King, S. M.; Leaf, P. A.; Olson, A. C.; Ray, P. Z.; Tarr, M. A. Photolytic and photocatalytic degradation of surface oil from the Deepwater Horizon spill. *Chemosphere* **2014**, *95* (0), 415−22.

(31) Radovic, J. R.; Aeppli, C.; Nelson, R. K.; Jimenez, N.; Reddy, C. M.; Bayona, J. M.; Albaiges, J. Assessment of photochemical processes in marine oil spill fingerprinting. *Mar. Pollut. Bull.* **2014**, *79* (1−2), 268−77.

(32) Faksness, L. G.; Altin, D.; Nordtug, T.; Daling, P. S.; Hansen, B. H. Chemical comparison and acute toxicity of water accommodated fraction (WAF) of source and field collected Macondo oils from the Deepwater Horizon spill. *Mar. Pollut. Bull.* **2015**, *91* (1), 222−9.

(33) Theurich, J.; Bahnemann, D. W.; Vogel, R.; Ehamed, F. E.; Alhakimi, G.; Rajab, I. Photocatalytic degradation of naphthalene and anthracene: GC-MS analysis of the degradation pathway. *Res. Chem. Intermed.* **1997**, *23* (3), 247−274.

(34) Rontani, J. F.; Giral, P. J. P. Significance of Photosensitized Oxidation of Alkanes during the Photochemical Degradation of Petroleum Hydrocarbon Fractions in Seawater. *Int. J. Environ. Anal. Chem.* **1990**, *42* (1−4), 61−68.

(35) Niederer, M. Determination of polycyclic aromatic hydro-carbons and substitutes (nitro-, Oxy-PAHs) in urban soil and airborne particulate by GC-MS and NCI-MS/MS. *Environ. Sci. Pollut. Res.* **1998**, *5* (4), 209−16.

(36) Poster, D. L.; Schantz, M. M.; Sander, L. C.; Wise, S. A. Analysis of polycyclic aromatic hydrocarbons (PAHs) in environmental samples: a critical review of gas chromatographic (GC) methods. *Anal. Bioanal. Chem.* **2006**, *386* (4), 859−81.

(37) Webb, P. J.; Hamilton, J. F.; Lewis, A. C.; Wirtz, K. Formation of oxygenated-polycyclic aromatic compounds in aerosol from the photo-oxidation of o-tolualdehyde. *Polycyclic Aromat. Compd.* **2006**, *26* (4), 237−252.

(38) McKenna, A. M.; Nelson, R. K.; Reddy, C. M.; Savory, J. J.; Kaiser, N. K.; Fitzsimmons, J. E.; Marshall, A. G.; Rodgers, R. P. Expansion of the analytical window for oil spill characterization by ultrahigh resolution mass spectrometry: beyond gas chromatography. *Environ. Sci. Technol.* **2013**, *47* (13), 7530−9.

(39) Forth, H. P.; Mitchelmore, C. L.; Morris, J. M.; Lipton, J. Characterization of oil and water accommodated fractions used to conduct aquatic toxicity testing in support of the Deepwater Horizon oil spill natural resource damage assessment. *Environ. Toxicol. Chem.* **2016**, DOI: 10.1002/etc.3672.

(40) Rowland, S.; Donkin, P.; Smith, E.; Wraige, E. Aromatic Hydrocarbon "Humps" in the Marine Environment: Unrecognized Toxins? *Environ. Sci. Technol.* **2001**, *35* (13), 2640−2644.

(41) Ray, P. Z.; Chen, H.; Podgorski, D. C.; McKenna, A. M.; Tarr, M. A. Sunlight creates oxygenated species in water-soluble fractions of Deepwater Horizon oil. *J. Hazard. Mater.* **2014**, *280* (0), 636−43.

(42) Ruddy, B. M.; Huettel, M.; Kostka, J. E.; Lobodin, V. V.; Bythell, B. J.; McKenna, A. M.; Aeppli, C.; Reddy, C. M.; Nelson, R. K.; Marshall, A. G.; Rodgers, R. P. Targeted Petroleomics: Analytical Investigation of Macondo Well Oil Oxidation Products from Pensacola Beach. *Energy Fuels* **2014**, *28* (6), 4043−4050.

(43) Griffiths, M. T.; Da Campo, R.; O'Connor, P. B.; Barrow, M. P. Throwing light on petroleum: simulated exposure of crude oil to sunlight and characterization using atmospheric pressure photo-ionization fourier transform ion cyclotron resonance mass spectrometry. *Anal. Chem.* **2014**, *86* (1), 527−34.

(44) Islam, A.; Cho, Y.; Yim, U. H.; Shim, W. J.; Kim, Y. H.; Kim, S. The comparison of naturally weathered oil and artificially photo-degraded oil at the molecular level by a combination of SARA fractionation and FT-ICR MS. *J. Hazard. Mater.* **2013**, *263* (Part 2), 404−411.

(45) Zhu, X.; Shi, Q.; Zhang, Y.; Pan, N.; Xu, C.; Chung, K. H.; Zhao, S. *Energy Fuels* **2011**, *25*, 281.

(46) Molnárné Guricza, L.; Schrader, W. Electrospray ionization for determination of non-polar polyaromatic hydrocarbons and poly-aromatic heterocycles in heavy crude oil asphaltenes. *J. Mass Spectrom.* **2015**, *50* (3), 549−557.

(47) Hourani, N.; Andersson, J. T.; Möller, I.; Amad, M. a.; Witt, M.; Sarathy, S. M. Atmospheric pressure chemical ionization Fourier transform ion cyclotron resonance mass spectrometry for complex thiophenic mixture analysis. *Rapid Commun. Mass Spectrom.* **2013**, *27* (21), 2432−2438.

(48) Barrow, M. P.; Peru, K. M.; Headley, J. V. An added dimension: GC atmospheric pressure chemical ionization FTICR MS and the Athabasca oil sands. *Anal. Chem.* **2014**, *86* (16), 8281−8288.

(49) Headley, J. V.; Peru, K. M.; Barrow, M. P. Advances in mass spectrometric characterization of naphthenic acids fraction compounds in oil sands environmental samples and crude oil—a review. *Mass Spectrom. Rev.* **2016**, *35* (2), 311−328.

(50) Headley, J. V.; Peru, K. M.; Mohamed, M. H.; Wilson, L.; McMartin, D. W.; Mapolelo, M. M.; Lobodin, V. V.; Rodgers, R. P.; Marshall, A. G. Atmospheric Pressure Photoionization Fourier Transform Ion Cyclotron Resonance Mass Spectrometry Character-ization of Tunable Carbohydrate-Based Materials for Sorption of Oil Sands Naphthenic Acids. *Energy Fuels* **2014**, *28* (3), 1611−1616.

(51) Bae, E.; Na, J.-G.; Chung, S. H.; Kim, H. S.; Kim, S. Identification of about 30 000 chemical components in shale oils by electrospray ionization (ESI) and atmospheric pressure photo-ionization (APPI) coupled with 15 T Fourier transform ion cyclotron resonance mass spectrometry (FT-ICR MS) and a comparison to conventional oil. *Energy Fuels* **2010**, *24* (4), 2563−2569.

(52) Corilo, Y. E.; Rowland, S. M.; Rodgers, R. P. Calculation of the total sulfur content in crude oils by positive-ion atmospheric pressure photoionization Fourier transform ion cyclotron resonance mass spectrometry. *Energy Fuels* **2016**, *30* (5), 3962−3966.

(53) Vetere, A.; Schrader, W. Mass Spectrometric Coverage of Complex Mixtures: Exploring the Carbon Space of Crude Oil. *ChemistrySelect* **2017**, *2* (3), 849−853.

(54) Stader, C.; Beer, F. T.; Achten, C. Environmental PAH analysis by gas chromatography−atmospheric pressure laser ionization−time-of-flight−mass spectrometry (GC-APLI-MS). *Anal. Bioanal. Chem.* **2013**, *405* (22), 7041−7052.

(55) Schmitt-Kopplin, P.; Englmann, M.; Rossello-Mora, R.; Schiewek, R.; Brockmann, K. J.; Benter, T.; Schmitz, O. J. Combining chip-ESI with APLI (cESILI) as a multimode source for analysis of complex mixtures with ultrahigh-resolution mass spectrometry. *Anal. Bioanal. Chem.* **2008**, *391* (8), 2803−2809.

(56) Schiewek, R.; Schellenträger, M.; Mönnikes, R.; Lorenz, M.; Giese, R.; Brockmann, K.; Gäb, S.; Benter, T.; Schmitz, O. Ultrasensitive determination of polycyclic aromatic compounds with atmospheric-pressure laser ionization as an interface for GC/MS. *Anal. Chem.* **2007**, *79* (11), 4135−4140.

(57) Streibel, T.; Zimmermann, R. Resonance-Enhanced Multi-photon Ionization Mass Spectrometry (REMPI-MS): Applications for Process Analysis. *Annu. Rev. Anal. Chem.* **2014**, *7* (1), 361−381.

(58) Gaspar, A.; Zellermann, E.; Lababidi, S.; Reece, J.; Schrader, W. Characterization of Saturates, Aromatics, Resins, and Asphaltenes Heavy Crude Oil Fractions by Atmospheric Pressure Laser Ionization Fourier Transform Ion Cyclotron Resonance Mass Spectrometry. *Energy Fuels* **2012**, *26* (6), 3481−3487.

(59) Lababidi, S.; Panda, S. K.; Andersson, J. T.; Schrader, W. Direct coupling of normal-phase high-performance liquid chromatography to atmospheric pressure laser ionization fourier transform ion cyclotron resonance mass spectrometry for the characterization of crude oil. *Anal. Chem.* **2013**, *85* (20), 9478−85.

(60) Lababidi, S.; Schrader, W. Online normal-phase high-perform-ance liquid chromatography/Fourier transform ion cyclotron reso-nance mass spectrometry: effects of different ionization methods on the characterization of highly complex crude oil mixtures. *Rapid Commun. Mass Spectrom.* **2014**, *28* (12), 1345−52.

(61) Panda, S. K.; Brockmann, K.-J.; Benter, T.; Schrader, W. Atmospheric pressure laser ionization (APLI) coupled with Fourier transform ion cyclotron resonance mass spectrometry applied to petroleum samples analysis: comparison with electrospray ionization and atmospheric pressure photoionization methods. *Rapid Commun. Mass Spectrom.* **2011**, *25* (16), 2317−2326.

(62) Huba, A. K.; Huba, K.; Gardinali, P. R. Understanding the atmospheric pressure ionization of petroleum components: The effects of size, structure, and presence of heteroatoms. *Sci. Total Environ.* **2016**, *568*, 1018−1025.

(63) Cho, Y.; Ahmed, A.; Islam, A.; Kim, S. Developments in FT-ICR MS instrumentation, ionization techniques, and data interpretation methods for petroleomics. *Mass Spectrom. Rev.* **2015**, *34* (2), 248−263.

(64) Pudenzi, M. A.; Eberlin, M. N. Assessing Relative Electrospray Ionization, Atmospheric Pressure Photoionization, Atmospheric Pressure Chemical Ionization, and Atmospheric Pressure Photo- and Chemical Ionization Efficiencies in Mass Spectrometry Petroleomic Analysis via Pools and Pairs of Selected Polar Compound Standards. *Energy Fuels* **2016**, *30* (9), 7125−7133.

(65) Benigni, P.; DeBord, J. D.; Thompson, C. J.; Gardinali, P.; Fernandez-Lima, F. Increasing Polyaromatic Hydrocarbon (PAH) Molecular Coverage during Fossil Oil Analysis by Combining Gas Chromatography and Atmospheric-Pressure Laser Ionization Fourier Transform Ion Cyclotron Resonance Mass Spectrometry (FT-ICR MS). *Energy Fuels* **2016**, *30* (1), 196−203.

(66) Molnárné Guricza, L.; Schrader, W. New Separation Approach for Asphaltene Investigation: Argentation Chromatography Coupled with Ultrahigh-Resolution Mass Spectrometry. *Energy Fuels* **2015**, *29* (10), 6224−6230.

(67) Ghislain, T.; Molnarne Guricza, L.; Schrader, W. Character-ization of crude oil asphaltenes by coupling size exclusion chromatography directly to an ultrahigh resolution mass spectrometer. *Rapid Commun. Mass Spectrom.* **2017**, *31* (6), 495−502.

(68) Ramirez, C. E.; Wang, C.; Gardinali, P. R. Fully automated trace level determination of parent and alkylated PAHs in environmental waters by online SPE-LC-APPI-MS/MS. *Anal. Bioanal. Chem.* **2014**, *406* (1), 329−344.

(69) Rüger, C. P.; Schwemer, T.; Sklorz, M.; O'Connor, P. B.; Barrow, M. P.; Zimmermann, R. Comprehensive chemical comparison of fuel composition and aerosol particles emitted from a ship diesel engine by gas chromatography atmospheric pressure chemical ionisation ultra-high resolution mass spectrometry with improved data processing routines. *Eur. J. Mass Spectrom* **2017**, *23* (1), 28−39.

(70) Vetere, A.; Schrader, W. 1-and 2-Photon ionization for online FAIMS-FTMS coupling allows new insights into the constitution of crude oils. *Anal. Chem.* **2015**, *87* (17), 8874−8879.

(71) Ibrahim, Y. M.; Garimella, S. V.; Prost, S. A.; Wojcik, R.; Norheim, R. V.; Baker, E. S.; Rusyn, I.; Smith, R. D. Development of an Ion Mobility Spectrometry-Orbitrap Mass Spectrometer Platform. *Anal. Chem.* **2016**, *88* (24), 12152−12160.

(72) Kailemia, M. J.; Park, M.; Kaplan, D. A.; Venot, A.; Boons, G. J.; Li, L.; Linhardt, R. J.; Amster, I. J. High-field asymmetric-waveform ion mobility spectrometry and electron detachment dissociation of isobaric mixtures of glycosaminoglycans. *J. Am. Soc. Mass Spectrom.* **2014**, *25* (2), 258−68.

(73) Robinson, E. W.; Garcia, D. E.; Leib, R. D.; Williams, E. R. Enhanced mixture analysis of poly(ethylene glycol) using high-field asymmetric waveform ion mobility spectrometry combined with fourier transform ion cyclotron resonance mass spectrometry. *Anal. Chem.* **2006**, *78* (7), 2190−8.

(74) Robinson, E. W.; Leib, R. D.; Williams, E. R. The role of conformation on electron capture dissociation of ubiquitin. *J. Am. Soc. Mass Spectrom.* **2006**, *17* (10), 1470−1479.

(75) Robinson, E. W.; Sellon, R. E.; Williams, E. R. Peak deconvolution in high-field asymmetric waveform ion mobility spectrometry (FAIMS) to characterize macromolecular conformations. *Int. J. Mass Spectrom.* **2007**, *259* (1–3), 87–95.

(76) Robinson, E. W.; Williams, E. R. Multidimensional separations of ubiquitin conformers in the gas phase: relating ion cross sections to H/D exchange measurements. *J. Am. Soc. Mass Spectrom.* **2005**, *16* (9), 1427–37.

(77) Tang, X.; Bruce, J. E.; Hill, H. H., Jr. Design and performance of an atmospheric pressure ion mobility Fourier transform ion cyclotron resonance mass spectrometer. *Rapid Commun. Mass Spectrom.* **2007**, *21* (7), 1115–22.

(78) Bluhm, B. K.; Gillig, K. J.; Russell, D. H. Development of a Fourier-transform ion cyclotron resonance mass spectrometer-ion mobility spectrometer. *Rev. Sci. Instrum.* **2000**, *71* (11), 4078–4086.

(79) Benigni, P.; Thompson, C. J.; Ridgeway, M. E.; Park, M. A.; Fernandez-Lima, F. Targeted high-resolution ion mobility separation coupled to ultrahigh-resolution mass spectrometry of endocrine disruptors in complex mixtures. *Anal. Chem.* **2015**, *87* (8), 4321–5.

(80) Wu, C.; Siems, W. F.; Asbury, G. R.; Hill, H. H. Electrospray Ionization High-Resolution Ion Mobility Spectrometry–Mass Spectrometry. *Anal. Chem.* **1998**, *70* (23), 4929–4938.

(81) Jarrold, M. F.; Constant, V. A. Silicon cluster ions: evidence for a structural transition. *Phys. Rev. Lett.* **1991**, *67* (21), 2994.

(82) Kanu, A. B.; Dwivedi, P.; Tam, M.; Matz, L.; Hill, H. H. Ion mobility–mass spectrometry. *J. Mass Spectrom.* **2008**, *43* (1), 1–22.

(83) Becker, C.; Qian, K.; Russell, D. H. Molecular Weight Distributions of Asphaltenes and Deasphaltened Oils Studied by Laser Desorption Ionization and Ion Mobility Mass Spectrometry. *Anal. Chem.* **2008**, *80* (22), 8592–8597.

(84) Lalli, P. M.; Corilo, Y. E.; Rowland, S. M.; Marshall, A. G.; Rodgers, R. P. Isomeric Separation and Structural Characterization of Acids in Petroleum by Ion Mobility Mass Spectrometry. *Energy Fuels* **2015**, *29* (6), 3626–3633.

(85) Fasciotti, M.; Lalli, P. M.; Klitzke, C. F.; Corilo, Y. E.; Pudenzi, M. A.; Pereira, R. C. L.; Bastos, W.; Daroda, R. J.; Eberlin, M. N. Petroleomics by Traveling Wave Ion Mobility-Mass Spectrometry Using CO2 as a Drift Gas. *Energy Fuels* **2013**, *27* (12), 7277–7286.

(86) Fernandez-Lima, F. A.; Becker, C.; McKenna, A. M.; Rodgers, R. P.; Marshall, A. G.; Russell, D. H. Petroleum crude oil characterization by IMS-MS and FTICR MS. *Anal. Chem.* **2009**, *81* (24), 9941–7.

(87) Becker, C.; Fernandez-Lima, F. A.; Russell, D. H. Ion Mobility-Mass Spectrometry: A Tool for Characterizing the Petroleome. *Spectroscopy* **2009**, *24* (4), 38–42.

(88) Ahmed, A.; Cho, Y.; Giles, K.; Riches, E.; Lee, J. W.; Kim, H. I.; Choi, C. H.; Kim, S. Elucidating Molecular Structures of Nonalkylated and Short-Chain Alkyl ($n < 5$, (CH2)n) Aromatic Compounds in Crude Oils by a Combination of Ion Mobility and Ultrahigh-Resolution Mass Spectrometries and Theoretical Collisional Cross-Section Calculations. *Anal. Chem.* **2014**, *86* (7), 3300–3307.

(89) Ahmed, A.; Cho, Y. J.; No, M.-h.; Koh, J.; Tomczyk, N.; Giles, K.; Yoo, J. S.; Kim, S. Application of the Mason–Schamp Equation and Ion Mobility Mass Spectrometry To Identify Structurally Related Compounds in Crude Oil. *Anal. Chem.* **2011**, *83* (1), 77–83.

(90) Farenc, M.; Corilo, Y. E.; Lalli, P. M.; Riches, E.; Rodgers, R. P.; Afonso, C.; Giusti, P. Comparison of Atmospheric Pressure Ionization for the Analysis of Heavy Petroleum Fractions with Ion Mobility-Mass Spectrometry. *Energy Fuels* **2016**, *30* (11), 8896–8903.

(91) Santos, J. M.; Galaverna, R. d. S.; Pudenzi, M. A.; Schmidt, E. M.; Sanders, N. L.; Kurulugama, R. T.; Mordehai, A.; Stafford, G. C.; Wisniewski, A.; Eberlin, M. N. Petroleomics by ion mobility mass spectrometry: resolution and characterization of contaminants and additives in crude oils and petrofuels. *Anal. Methods* **2015**, *7* (11), 4450–4463.

(92) Lalli, P. M.; Jarvis, J. M.; Marshall, A. G.; Rodgers, R. P. Functional Isomers in Petroleum Emulsion Interfacial Material Revealed by Ion Mobility Mass Spectrometry and Collision-Induced Dissociation. *Energy Fuels* **2017**, *31* (1), 311–318.

(93) Hernandez, D. R.; Debord, J. D.; Ridgeway, M. E.; Kaplan, D. A.; Park, M. A.; Fernandez-Lima, F. Ion dynamics in a trapped ion mobility spectrometer. *Analyst* **2014**, *139* (8), 1913–21.

(94) Fernandez-Lima, F. A.; Kaplan, D. A.; Park, M. A. Note: Integration of trapped ion mobility spectrometry with mass spectrometry. *Rev. Sci. Instrum.* **2011**, *82* (12), 126106.

(95) Fernandez-Lima, F.; Kaplan, D. A.; Suetering, J.; Park, M. A. Gas-phase separation using a trapped ion mobility spectrometer. *Int. J. Ion Mobility Spectrom.* **2011**, *14* (2–3), 93–98.

(96) Castellanos, A.; Benigni, P.; Hernandez, D. R.; DeBord, J. D.; Ridgeway, M. E.; Park, M. A.; Fernandez-Lima, F. Fast Screening of Polycyclic Aromatic Hydrocarbons using Trapped Ion Mobility Spectrometry - Mass Spectrometry. *Anal. Methods* **2014**, *6* (23), 9328–9332.

(97) Benigni, P.; Marin, R.; Fernandez-Lima, F. Towards unsupervised polyaromatic hydrocarbons structural assignment from SA-TIMS–FTMS data. *Int. J. Ion Mobility Spectrom.* **2015**, *18* (3), 151–157.

(98) Schenk, E. R.; Mendez, V.; Landrum, J. T.; Ridgeway, M. E.; Park, M. A.; Fernandez-Lima, F. Direct observation of differences of carotenoid polyene chain cis/trans isomers resulting from structural topology. *Anal. Chem.* **2014**, *86* (4), 2019–24.

(99) Schenk, E. R.; Ridgeway, M. E.; Park, M. A.; Leng, F.; Fernandez-Lima, F. Isomerization kinetics of AT hook decapeptide solution structures. *Anal. Chem.* **2014**, *86* (2), 1210–4.

(100) Schenk, E. R.; Nau, F.; Fernandez-Lima, F. Theoretical predictor for candidate structure assignment from IMS data of biomolecule-related conformational space. *Int. J. Ion Mobility Spectrom.* **2015**, *18* (1), 23–29.

(101) Schenk, E. R.; Almeida, R.; Miksovska, J.; Ridgeway, M. E.; Park, M. A.; Fernandez-Lima, F. Kinetic intermediates of holo- and apo-myoglobin studied using HDX-TIMS-MS and molecular dynamic simulations. *J. Am. Soc. Mass Spectrom.* **2015**, *26* (4), 555–63.

(102) Benigni, P.; Marin, R.; Molano-Arevalo, J. C.; Garabedian, A.; Wolff, J. J.; Ridgeway, M. E.; Park, M. A.; Fernandez-Lima, F. Towards the Analysis of High Molecular Weight Proteins and Protein complexes using TIMS-MS. *Int. J. Ion Mobility Spectrom.* **2016**, *19* (2), 95–104.

(103) Garabedian, A.; Butcher, D.; Lippens, J. L.; Miksovska, J.; Chapagain, P. P.; Fabris, D.; Ridgeway, M. E.; Park, M. A.; Fernandez-Lima, F. Structures of the kinetically trapped i-motif DNA intermediates. *Phys. Chem. Chem. Phys.* **2016**, *18* (38), 26691–26702.

(104) Molano-Arevalo, J. C.; Hernandez, D. R.; Gonzalez, W. G.; Miksovska, J.; Ridgeway, M. E.; Park, M. A.; Fernandez-Lima, F. Flavin adenine dinucleotide structural motifs: from solution to gas phase. *Anal. Chem.* **2014**, *86* (20), 10223–30.

(105) McKenzie-Coe, A.; DeBord, J. D.; Ridgeway, M.; Park, M.; Eiceman, G.; Fernandez-Lima, F. Lifetimes and stabilities of familiar explosive molecular adduct complexes during ion mobility measurements. *Analyst* **2015**, *140* (16), 5692–9.

(106) Benigni, P.; Fernandez-Lima, F. Oversampling Selective Accumulation Trapped Ion Mobility Spectrometry Coupled to FT-ICR MS: Fundamentals and Applications. *Anal. Chem.* **2016**, *88* (14), 7404–12.

(107) Adams, K. J.; Montero, D.; Aga, D.; Fernandez-Lima, F. Isomer separation of polybrominated diphenyl ether metabolites using nanoESI-TIMS-MS. *Int. J. Ion Mobility Spectrom.* **2016**, *19* (2), 69–76.

(108) Silveira, J. A.; Ridgeway, M. E.; Laukien, F. H.; Mann, M.; Park, M. A. Parallel accumulation for 100% duty cycle trapped ion mobility-mass spectrometry. *Int. J. Mass Spectrom.* **2017**, *413*, 168–175.

(109) Michelmann, K.; Silveira, J. A.; Ridgeway, M. E.; Park, M. A. Fundamentals of Trapped Ion Mobility Spectrometry. *J. Am. Soc. Mass Spectrom.* **2015**, *26* (1), 14–24.

(110) Silveira, J. A.; Michelmann, K.; Ridgeway, M. E.; Park, M. A. Fundamentals of Trapped Ion Mobility Spectrometry Part II: Fluid Dynamics. *J. Am. Soc. Mass Spectrom.* **2016**, *27* (4), 585–595.

(111) Silveira, J. A.; Danielson, W.; Ridgeway, M. E.; Park, M. A. Altering the mobility-time continuum: nonlinear scan functions for

targeted high resolution trapped ion mobility-mass spectrometry. *Int. J. Ion Mobility Spectrom.* **2016**, *19* (2), 87−94.

(112) Ridgeway, M. E.; Silveira, J. A.; Meier, J. E.; Park, M. A. Microheterogeneity within conformational states of ubiquitin revealed by high resolution trapped ion mobility spectrometry. *Analyst* **2015**, *140* (20), 6964−6972.

(113) Meier, F.; Beck, S.; Grassl, N.; Lubeck, M.; Park, M. A.; Raether, O.; Mann, M. Parallel Accumulation−Serial Fragmentation (PASEF): Multiplying Sequencing Speed and Sensitivity by Synchronized Scans in a Trapped Ion Mobility Device. *J. Proteome Res.* **2015**, *14* (12), 5378−5387.

(114) Silveira, J. A.; Ridgeway, M. E.; Park, M. A. High Resolution Trapped Ion Mobility Spectrometery of Peptides. *Anal. Chem.* **2014**, *86* (12), 5624−5627.

(115) Ridgeway, M. E.; Wolff, J. J.; Silveira, J. A.; Lin, C.; Costello, C. E.; Park, M. A. Gated trapped ion mobility spectrometry coupled to fourier transform ion cyclotron resonance mass spectrometry. *Int. J. Ion Mobility Spectrom.* **2016**, *19* (2), 77−85.

(116) Pu, Y.; Ridgeway, M. E.; Glaskin, R. S.; Park, M. A.; Costello, C. E.; Lin, C. Separation and Identification of Isomeric Glycans by Selected Accumulation-Trapped Ion Mobility Spectrometry-Electron Activated Dissociation Tandem Mass Spectrometry. *Anal. Chem.* **2016**, *88* (7), 3440−3443.

(117) Liu, F. C.; Kirk, S. R.; Bleiholder, C. On the structural denaturation of biological analytes in trapped ion mobility spectrometry−mass spectrometry. *Analyst* **2016**, *141* (12), 3722−3730.

(118) Lundstedt, S.; White, P. A.; Lemieux, C. L.; Lynes, K. D.; Lambert, L. B.; Oberg, L.; Haglund, P.; Tysklind, M. Sources, fate, and toxic hazards of oxygenated polycyclic aromatic hydrocarbons (PAHs) at PAH-contaminated sites. *Ambio* **2007**, *36* (6), 475−485.

(119) Singer, M. M.; Aurand, D.; Bragin, G. E.; Clark, J. R.; Coelho, G. M.; Sowby, M. L.; Tjeerdema, R. S. Standardization of the preparation and quantitation of water-accommodated fractions of petroleum for toxicity testing. *Mar. Pollut. Bull.* **2000**, *40* (11), 1007−1016.

(120) Benigni, P.; Marin, R.; Sandoval, K.; Gardinali, P.; Fernandez-Lima, F. Chemical Analysis of Water-accommodated Fractions of Crude Oil Spills Using TIMS-FT-ICR MS. *J. Visualized Exp.* **2017**, *121*, e55352.

(121) McDaniel, E. W.; Mason, E. A. *Mobility and diffusion of ions in gases*; John Wiley and Sons, Inc.: New York, New York, 1973; p 381.

(122) Savory, J. J.; Kaiser, N. K.; McKenna, A. M.; Xian, F.; Blakney, G. T.; Rodgers, R. P.; Hendrickson, C. L.; Marshall, A. G. Parts-per-billion Fourier transform ion cyclotron resonance mass measurement accuracy with a "walking" calibration equation. *Anal. Chem.* **2011**, *83* (5), 1732−1736.

(123) Du, P.; Kibbe, W. A.; Lin, S. M. Improved peak detection in mass spectrum by incorporating continuous wavelet transform-based pattern matching. *Bioinformatics* **2006**, *22* (17), 2059−2065.

(124) Oliphant, T. E. Python for Scientific Computing. *Comput. Sci. Eng.* **2007**, *9* (3), 10−20.

(125) Moré, J. J.; Garbow, B. S.; Hillstrom, K. E. *User guide for MINPACK-1*; CM-P00068642; 1980.

(126) Hunter, J. D. Matplotlib: A 2D graphics environment. *Comput. Sci. Eng.* **2007**, *9* (3), 90−95.

(127) Fasciotti, M.; Lalli, P. M.; Heerdt, G.; Steffen, R. A.; Corilo, Y. E.; de Sá, G. F.; Daroda, R. J.; Reis, F. d. A. M.; Morgon, N. H.; Pereira, R. C. L.; Eberlin, M. N.; Klitzke, C. F. Structure-drift time relationships in ion mobility mass spectrometry. *Int. J. Ion Mobility Spectrom.* **2013**, *16* (2), 117−132.

(128) Dabestani, R.; Ivanov, I. N. A compilation of physical, spectroscopic and photophysical properties of polycyclic aromatic hydrocarbons. *Photochem. Photobiol.* **1999**, *70* (1), 10−34.

(129) Chen, H.; Hou, A.; Corilo, Y. E.; Lin, Q.; Lu, J.; Mendelssohn, I. A.; Zhang, R.; Rodgers, R. P.; McKenna, A. M. 4 Years after the Deepwater Horizon Spill: Molecular Transformation of Macondo Well Oil in Louisiana Salt Marsh Sediments Revealed by FT-ICR Mass Spectrometry. *Environ. Sci. Technol.* **2016**, *50* (17), 9061−9069.

(130) Leshuk, T.; Wong, T.; Linley, S.; Peru, K. M.; Headley, J. V.; Gu, F. Solar photocatalytic degradation of naphthenic acids in oil sands process-affected water. *Chemosphere* **2016**, *144*, 1854−1861.

(131) Huba, A. K.; Gardinali, P. R. Characterization of a crude oil weathering series by ultrahigh-resolution mass spectrometry using multiple ionization modes. *Sci. Total Environ.* **2016**, *563−564*, 600−610.

(132) van Agthoven, M. A.; Delsuc, M.-A.; Rolando, C. Two-dimensional FT-ICR/MS with IRMPD as fragmentation mode. *Int. J. Mass Spectrom.* **2011**, *306* (2), 196−203.

(133) Laskin, J. Energy and Entropy Effects in Gas-Phase Dissociation of Peptides and Proteins. In *Principles of Mass Spectrometry Applied to Biomolecules*; John Wiley & Sons, Inc.: 2006; pp 619−665, DOI: 10.1002/047005042X.ch16.

(134) Klassen, J. S.; Schnier, P. D.; Williams, E. R. Blackbody infrared radiative dissociation of oligonucleotide anions. *J. Am. Soc. Mass Spectrom.* **1998**, *9* (11), 1117−24.

(135) Felitsyn, N.; Kitova, E. N.; Klassen, J. S. Thermal decomposition of a gaseous multiprotein complex studied by blackbody infrared radiative dissociation. Investigating the origin of the asymmetric dissociation behavior. *Anal. Chem.* **2001**, *73* (19), 4647−61.

(136) Dunbar, R. C. BIRD (blackbody infrared radiative dissociation): evolution, principles, and applications. *Mass Spectrom. Rev.* **2004**, *23* (2), 127−58.

(137) Yan, J.; Zhou, M.; Gilbert, J. D.; Wolff, J. J.; Somogyi, A.; Pedder, R. E.; Quintyn, R. S.; Morrison, L. J.; Easterling, M. L.; Paša-Tolić, L. Surface-induced dissociation (SID) of protein complexes in a hybrid Fourier transform ion cyclotron resonance (FT-ICR) mass spectrometer. *Anal. Chem.* **2017**, *89* (1), 895−901.

(138) Qi, Y.; Volmer, D. A. Structural analysis of small to medium-sized molecules by mass spectrometry after electron-ion fragmentation (ExD) reactions. *Analyst* **2016**, *141* (3), 794−806.